DOUBLE-SLOT ANTENNAS ON EXTENDED HEMISPHERICAL SILICON LENSES–GENERAL TREATMENT

George V. Eleftheriades and Gabriel M. Rebeiz

NASA/Center for Space Terahertz Technology
Electrical Engineering and Computer Science Department
University of Michigan
Ann Arbor, MI 48109-2122

I. PATTERNS OF AN EXTENDED SILICON LENS FED BY AN ELEMENTARY ANTENNA

Consider the extended hemispherical lens of figure (1) which is fed by an elementary antenna located at $(x_o, y_o, -L)$, with respect to the center of the hemisphere (origin). The hemispherical surface is assumed to lie in the far-field of the elementary antenna, so that ray-optics can be used in order to determine the surface fields. Once the fields transmitted just outside the hemispherical surface have been determined, equivalent electric and magnetic surface currents can also be specified. The far-field patterns of the lens system can then be constructed using simple diffraction theory, namely:

$$E_\theta = -\frac{jk\exp(-jkr)}{4\pi r}(L_\phi + \eta N_\theta) \quad (1)$$

$$E_\phi = \frac{jk\exp(-jkr)}{4\pi r}(L_\theta - \eta N_\phi) \quad (2)$$

where η is the intrinsic impedance of free-space.

The radiation vectors $\bar{N}$ and $\bar{L}$ appearing above are defined in terms of the equivalent electric $\bar{J}_s$ and magnetic currents $\bar{M}_s$ as follows:

$$\bar{N} = \int\int_{s'} \bar{J}_s \exp(jkR\cos(\psi))ds' \quad (3)$$

$$\bar{L} = \int\int_{s'} \bar{M}_s \exp(jkR\cos(\psi))ds' \quad (4)$$

where s' denotes the hemispherical surface, k is the free-space wavenumber, and r is the distance from the origin to the observation point. Furthermore, ψ is the angle between $\bar{r}$ and $\bar{r}'$ given by:

$$\cos(\psi) = \sin\theta\sin(\theta')\cos(\phi - \phi') + \cos(\theta)\cos(\theta') \quad (5)$$

As usually, the equivalent electric $\bar{J}_s$ and magnetic $\bar{M}_s$ currents are determined by:

$$\text{Electric Current} : \bar{J}_s = \hat{r}' \times \bar{H}_{tr} \quad (6)$$

$$\text{Magnetic Current} : \bar{M}_s = -\hat{r}' \times \bar{E}_{tr} \quad (7)$$

I.1 Definitions

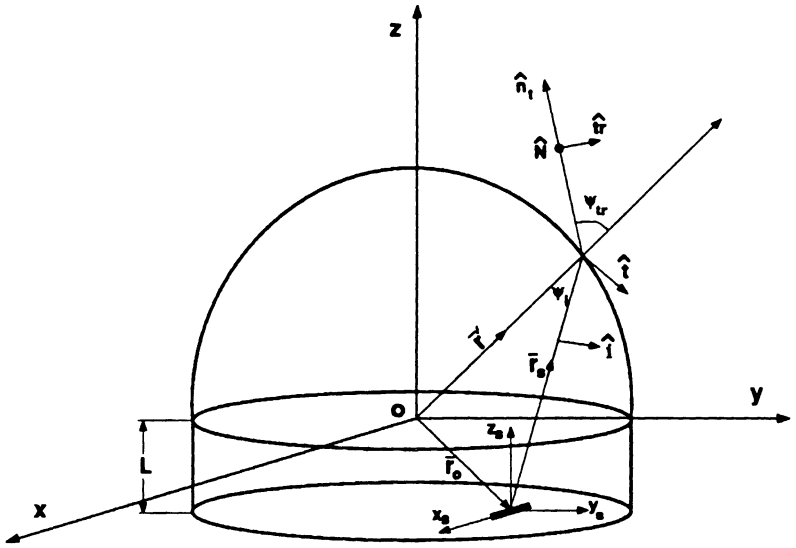

Figure 1: An extended hemispherical lens fed by an elementary antenna.

Hemispherical radius : R
Extension length : L
Location of elementary antenna: $\bar{r}_o = (x_o, y_o, -L)$
Normal to the hemispherical surface: $\hat{r}'$
Obsrvation point at far-field: (r, θ, ϕ)
Integration point on hemispherical surface: (r', θ', ϕ')
Integration point with respect to the elementary antenna: (r_s, θ_s, ϕ_s)
Direction of propagation of incident field: $\hat{r}_s$
Direction of propagation of transmitted field: $\hat{n}_t$
Plane of incidence: defined by $(\bar{r}', \bar{r}_s)$
Normal to plane of incidence: $\hat{N} = (\hat{r}_s \times \hat{r}')/\sin(\psi_i)$
Tangential to hemispherical surface included in plane of incidence: $\hat{t}$
Angle of incidence: ψ_i
Angle of transmission: ψ_{tr}
Polarization of parallel transmitted field: $\hat{tr}$
Polarization of perpendicular transmitted field: $\hat{N}$
Polarization of parallel incident field: $\hat{i}$
$(\hat{r}', \hat{t}, \hat{N})$: Right-handed basis in plane of incidence.
$(\hat{n}_t, \hat{tr}, \hat{N})$: Right-handed basis in plane of incidence.

With these definitions the right-handed basis $(\hat{r}', \hat{t}, \hat{N})$ is explicitly determined by:

$$\hat{r}' = R\sin(\theta')\cos(\phi')\hat{x} + R\sin(\theta')\sin(\phi')\hat{y} + \cos(\theta')\hat{z} \tag{8}$$

$$\begin{aligned}
\hat{t} &= t_x\hat{x} + t_y\hat{y} + t_z\hat{z} \qquad (9)\\
t_x &= \Big\{\cos(\phi')\cos(\theta_s)\sin(\theta')\cos(\theta') - \cos(\phi_s)\sin(\theta_s)\cos^2(\theta')\\
&- \sin(\phi')(\sin(\theta_s)\sin(\phi' - \phi_s)\sin^2(\theta'))\Big\} / \sin(\psi_i)\\
t_y &= \Big\{\cos(\phi')\sin^2(\theta')\sin(\theta_s)\sin(\phi' - \phi_s) - \cos^2(\theta')\sin\phi_s\sin(\theta_s)\\
&+ \sin(\phi')\sin(\theta')\cos(\theta')\cos(\theta_s)\Big\} / \sin(\psi_i)\\
t_z &= \Big\{-\sin^2(\theta')\cos(\theta_s) + \sin(\theta')\cos(\theta')\sin(\theta_s)\cos(\phi_s - \phi')\Big\} / \sin(\psi_i)
\end{aligned}$$

$$\begin{aligned}
\hat{N} &= N_x\hat{x} + N_y\hat{y} + N_z\hat{z} \qquad (10)\\
N_x &= \Big\{\cos(\theta')\sin(\theta_s)\sin(\phi_s) - \sin(\theta')\sin(\phi')\cos(\theta_s)\Big\} / \sin(\psi_i)\\
N_y &= \Big\{\sin(\theta')\cos(\phi')\cos(\theta_s) - \cos(\theta')\sin(\theta_s)\cos(\phi_s)\Big\} / \sin(\psi_i)\\
N_z &= \Big\{\sin(\phi' - \phi_s)\sin(\theta_s)\sin(\theta')\Big\} / \sin(\psi_i)
\end{aligned}$$

Furthermore, the orthonormal basis system $(\hat{n}_t, \hat{tr}, \hat{N})$ can be expressed in terms of $(\hat{r}', \hat{t}, \hat{N})$ by :

$$\hat{n}_t = \cos(\psi_{tr})\hat{r}' - \sin(\psi_{tr})\hat{t} \tag{11}$$

$$\hat{tr} = \sin(\psi_{tr})\hat{r}' + \cos(\psi_{tr})\hat{t} \tag{12}$$

Finally, the angle of incidence ψ_i, which is the angle between $\bar{r}'$ and $\bar{r}_s$, is determined by:

$$\cos(\psi_i) = \sin(\theta')\sin(\theta_s)\cos(\phi' - \phi_s) + \cos(\theta')\cos(\theta_s) \tag{13}$$

I.2 Equivalent Surface Currents

The equivalent currents flowing on the hemispherical surface have been defined in terms of the transmitted surface currents in equations (6) and (7). The transmitted surface fields can now be decomposed in terms of their parrallel and perpendicular components to the plane of incidence:

$$\bar{E}_{tr} = E_{tr,\parallel}\hat{tr} + E_{tr,\perp}\hat{N} \tag{14}$$

$$\eta\bar{H}_{tr} = \hat{n}_t \times \bar{E}_{tr} \tag{15}$$

Since we have available the expressions (8) to (10) for the unit vectors involved in the definitions of the equivalent surface currents we can explicitly write for the equivalent currents:

$$\begin{aligned} \eta \bar{J}_s &= -(\hat{t} E_{tr,\parallel} + \hat{N} \cos(\psi_{tr}) E_{tr,\perp}) && (16) \\ \bar{M}_s &= E_{tr,\perp} \hat{t} - E_{tr,\parallel} \cos(\psi_{tr}) \hat{N} && (17) \\ \text{and} \quad \cos(\psi_{tr}) &= \sqrt{1 - \epsilon_r \sin(\psi_i)^2} \end{aligned}$$

In order to explicitly determine the transmitted to the hemispherical surface fields we use ray-optics as was mentioned before. For this purpose, the elementary antenna fields should also be decomposed in their parallel and perpendicular components to the plane of incidence:

$$\begin{aligned} \bar{E}_s &= E_{s,\parallel} \hat{i} + E_{s,\perp} \hat{N} \\ \text{where} \quad \hat{i} &= \cos(\psi_i) \hat{t} + \sin(\psi_i) \hat{r}'. && (18) \end{aligned}$$

Given the elementary antenna fields, ray-optics determines the transmitted surface fields by:

$$\begin{aligned} E_{tr,\parallel} &= E_{s,\parallel} T_\parallel && (19) \\ E_{tr,\perp} &= E_{s,\perp} T_\perp && (20) \end{aligned}$$

where the parallel and perpendicular transmission coefficients $T_\parallel$ and $T_\perp$ are given by:

$$\begin{aligned} T_\parallel &= (1 + \Gamma_\parallel) \frac{\cos(\psi_i)}{\cos(\psi_{tr})} && (21) \\ T_\perp &= (1 + \Gamma_\perp) && (22) \\ \Gamma_\parallel &= \frac{\sqrt{\epsilon_r} \cos(\psi_{tr}) - \cos(\psi_i)}{\sqrt{\epsilon_r} \cos(\psi_{tr}) + \cos(\psi_i)} \\ \Gamma_\perp &= \frac{\sqrt{\epsilon_r} \cos(\psi_i) - \cos(\psi_{tr})}{\sqrt{\epsilon_r} \cos(\psi_i) + \cos(\psi_{tr})}. \end{aligned}$$

In general, the far-fields of the elementary antenna, with respect to its local coordinate system which is assumed to be parallel to the global one (see fig. 1), are of the form:

$$\begin{aligned} \bar{E}_s &= \frac{e^{-jk_d r_s}}{4\pi r_s} \left[g_{\theta s}(\theta_s, \phi_s) \hat{\theta}_s + g_{\phi s}(\theta_s, \phi_s) \hat{\phi}_s \right] && (23) \\ \eta_d \bar{H}_s &= \hat{r}_s \times \bar{E}_s && (24) \end{aligned}$$

where the subscript d indicates dielectric quantities, i.e. k_d and η_d are the dielectric wavenumber and intrinsinc dielectric impedance respectively. Using (18) and (23) the parallel and perpendicular electric field components of the elementary antenna are thus determined by:

$$\begin{aligned} E_{s,\parallel} &= \frac{e^{-jk_d r_s}}{4\pi r_s}\left\{g_{\theta s}\left[\cos(\psi_i)(\hat{\theta}_s\cdot\hat{t})+\sin(\psi_i)(\hat{\theta}_s\cdot\hat{r}')\right]\right. \\ &+ \left. g_{\phi s}\left[\cos(\psi_i)(\hat{\phi}_s\cdot\hat{t})+\sin(\psi_i)(\hat{\phi}_s\cdot\hat{r}')\right]\right\} \qquad (25) \\ E_{s,\perp} &= \frac{e^{-jk_d r_s}}{4\pi r_s}\left[g_{\theta s}(\hat{\theta}_s\cdot\hat{N})+g_{\phi s}(\hat{\phi}_s\cdot\hat{N})\right] \qquad (26) \end{aligned}$$

The dot products between the unit vectors appearing in (25) and (26) are computed by utilizing Cartesian coordinates:

$$\begin{aligned} \hat{\theta}_s\cdot\hat{t} &= t_x\cos(\theta_s)\cos(\phi_s)+t_y\cos(\theta_s)\sin(\phi_s)-t_z\sin(\theta_s) \qquad (27)\\ \hat{\theta}_s\cdot\hat{r}' &= \cos(\theta_s)\sin(\theta')\cos(\phi'-\phi_s)-\sin(\theta_s)\cos(\theta') \qquad (28)\\ \hat{\phi}_s\cdot\hat{t} &= -t_x\sin(\phi_s)+t_y\cos(\phi_s) \qquad (29)\\ \hat{\phi}_s\cdot\hat{r}' &= \sin(\theta')\sin(\phi'-\phi_s) \qquad (30)\\ \hat{\theta}_s\cdot\hat{N} &= N_x\cos(\theta_s)\cos(\phi_s)+N_y\cos(\theta_s)\sin(\phi_s)-N_z\sin(\theta_s) \qquad (31)\\ \hat{\phi}_s\cdot\hat{N} &= -N_x\sin(\phi_s)+N_y\cos(\phi_s). \qquad (32) \end{aligned}$$

Furthermore, since the equivalent surface currents in (3) and (4) are integrated with respect to the primed coordinates, the local to the elementary antenna coordinates should be converted to the primed coordinates using:

$$\bar{r}' = \bar{r}_s + \bar{r}_o \qquad (33)$$

I.3 Scattering Integrals

Once the equivalent surface currents have been determined as shown in the previous section, the far-field patterns can be obtained from equations (1) to (4). The resulting expression are as shown below:

$$\begin{aligned} E_\theta &= \frac{-jke^{-jkr}}{4\pi r}\int\int_{s'}(-E_{tr,\parallel}f_1+E_{tr,\perp}f_2)\,e^{jkR\cos\psi}\,ds' \qquad (34)\\ E_\phi &= \frac{jke^{-jkr}}{4\pi r}\int\int_{s'}(E_{tr,\parallel}f_2+E_{tr,\perp}f_1)\,e^{jkR\cos\psi}\,ds' \qquad (35) \end{aligned}$$

where

$$\begin{aligned} f_1 &= (\hat{\theta}\cdot\hat{t})+(\hat{\phi}\cdot\hat{N})\cos(\psi_{tr})\\ f_2 &= (\hat{\phi}\cdot\hat{t})-(\hat{\theta}\cdot\hat{N})\cos(\psi_{tr}) \end{aligned}$$

The dot products between the unit vectors appearing in (34) and (35) are given by expression similar to those of (27) to (32).

In the special case in which the lens is fed by a pair of parallel to the x-axis slots (see fig 2), the radiated elementary fields of (23) and (24) are defined by:

$$g_{\theta s} = g(\theta_s, \phi_s)(AF) \tag{36}$$

$$g_{\phi s} = g(\theta_s, \phi_s)\cos(\theta_s)\cos(\phi_s)(AF) \tag{37}$$

$$\text{and } g(\theta_s, \phi_s) = \frac{\cos(k_m l) - \cos(k_d l \sin(\theta_s)\cos(\phi_s))}{k_d^2 \sin(\theta_s)^2 \cos(\phi_s)^2 - k_m^2}$$

$$\text{Array-factor } : AF = \cos\left(k_d \frac{s}{2} \sin(\theta_s)\sin(\phi_s)\right)$$

$$\text{also } k_d = k\sqrt{\epsilon_r},\quad k_m = (k + k_d)/2$$

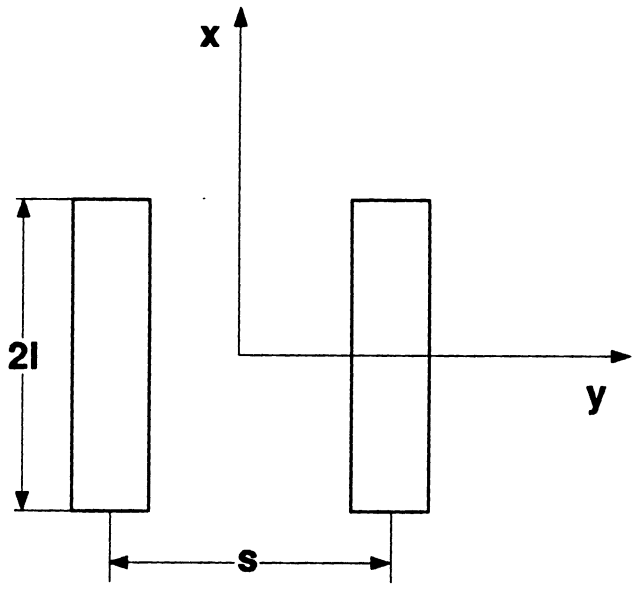

Figure 2: A pair of slot antennas feeding the lens.

II. COUPLING TO AN INCIDENT-BEAM

Assume that a beam with fields $(\bar{E}_G, \bar{H}_G)$ is incident on the lens, then the coupling efficiency η_G is defined as the ratio of the power incident to the power received by the elementary antenna, under matched conditions. The coupling efficiency can be computed by applying the reciprocity theorem in the form:

$$\oint_A (\bar{E}_{tr} \times \bar{H}_{tr} - \bar{E}_G \times \bar{H}_G) \cdot d\bar{A} = 0. \tag{38}$$

For our purposes we choose the surface A to consist of two parts, a spherical surface that just touches the lens and a smaller spherical surface that just touches the elementary antenna. By neglecting the power radiated at the back of the lens, one can proceed in a fashion similar to [1] and prove that η_G is given by:

$$\eta_G = \frac{1}{4} \frac{\left| \int \int_{s'} (\bar{E}_{tr} \times \bar{H}_G - \bar{E}_G \times \bar{H}_{tr}) \cdot \hat{r}' ds' \right|^2}{\left(\int \int_{s'} (\bar{E}_G \times \bar{H}_G^*) \cdot \hat{r}' ds' \right) \left(\int \int_{s'} (\bar{E}_{tr} \times \bar{H}_{tr}^*) \cdot \hat{r}' ds' \right)} \tag{39}$$

It should be noted here, that if the first part of the surface A in (38) is chosen to be a spherical surface in the far-field zone, as originally assumed in [1], then the integrand in the numerator of (39) can be simplified to just the dot product: $(2 * \bar{E} \cdot \bar{E}_G)$. However in such a case, the far-fields $\bar{E}$ need to be computed using equations (1) to (4), thus leading to quadruple integrals. Therefore, we prefer to employ the coupling form of (39) in which all the integrations are performed on the hemispherical surface s' and avoid quadruple integrals.

II.1 Coupling to a Gaussian beam

With reference to the geometry of fig. (3), an incident fundamental Gaussian beam in the $y - z$ plane, making an angle θ_o with the z-axis, will be of the form:

$$\bar{E}_G = \hat{\theta}_o \, g(x, y, z) \tag{40}$$

$$= \hat{\theta}_o \left(\frac{w_o}{w(z'')} \right) \exp(jkz'') \exp\left[j \frac{k}{2R(z'')} (x^2 + y_r^2) \right] \exp\left[\frac{x^2 + y_r^2}{w(z'')^2} \right]$$

$$\bar{H}_G = \hat{x} \, \frac{g(x, y, z)}{\eta} \tag{41}$$

where,

$$\text{Polarization: } \hat{\theta}_o = \hat{y}\cos(\theta_o) - \hat{z}\sin(\theta_o) \tag{42}$$

$$z'' = z_g + z_r \tag{43}$$

$$\text{Distance from origin: } z_r = z\ \cos(\theta_o) + y\ \sin(\theta_o) \tag{44}$$

$$\text{Axial distance: } y_r = y\ \cos(\theta_o) - z\ \sin(\theta_o) \tag{45}$$

$$\text{Waist radius: } w(z'') = w_o\left[1 + (\frac{z''}{z_c})^2\right]^{1/2} \tag{46}$$

$$\text{Radius of curvuture: } = z''\left[1 + (\frac{z_c}{z''})^2\right] \tag{47}$$

$$\frac{z''}{z_c} = \frac{\lambda z''}{\pi w_o^2} \tag{48}$$

z_g is the location of the beam waist behind the origin and w_o is the corresponding waist radius.

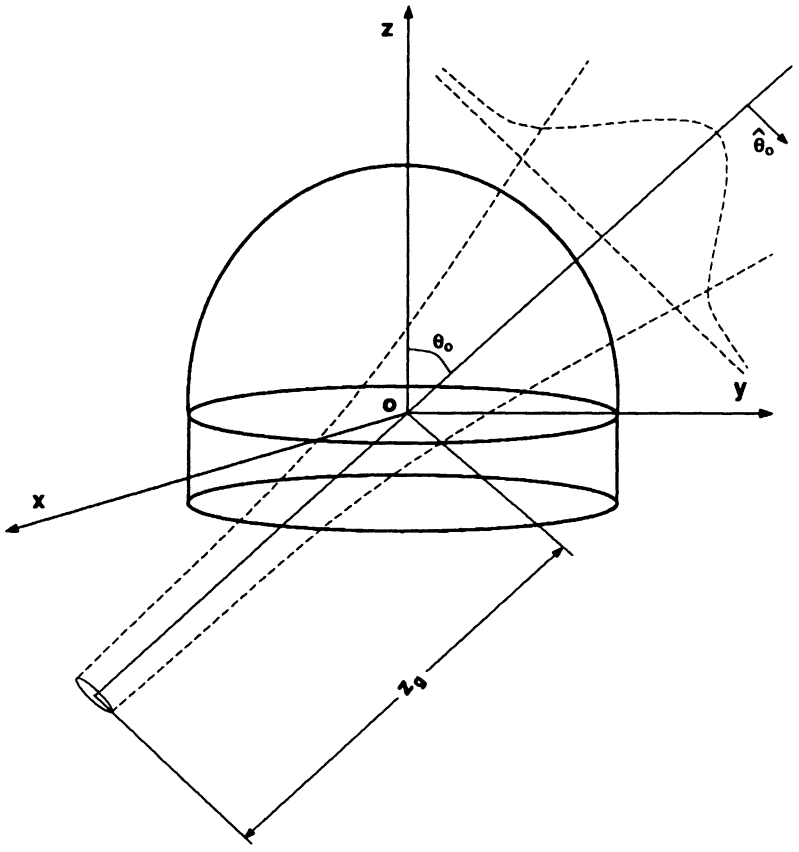

Figure 3: An incident Gaussian beam in the $y-z$-plane.

For the Gaussian beam described by (40) and (41) we can use the transmitted

field expressions of (14) and (15) in the coupling efficiency expression of (39) to obtain:

$$\eta_g = \frac{1}{4}\frac{|P_{cp}|^2}{(P_G)(P_{tr})} \tag{49}$$

where

$$\begin{aligned} P_{cp} &= \int_0^{2\pi}\int_0^{\pi/2} g(r')\{\bar{E}_{tr,\parallel}[\cos(\theta_o)t_y - \sin(\theta_o)t_z - N_x\cos(\psi_{tr})] \\ &+ \bar{E}_{tr,\perp}[(\cos(\theta_o)N_y - \sin(\theta_o)N_z)\cos(\psi_{tr}) + t_x]\}\, ds' \end{aligned} \tag{50}$$

$$P_G = \int_0^{2\pi}\int_0^{\pi/2}\left(\frac{w_o}{w}\right)^2 \exp\left(-2\frac{x'^2+y_r^2}{w^2}\right)(\sin(\theta_o)\sin(\theta')\cos(\phi') + \cos(\theta_o)\cos(\theta'))\, ds'$$

$$P_{tr} = \int_0^{2\pi}\int_0^{\pi/2}(|\bar{E}_{tr,\parallel}|^2 + |\bar{E}_{tr,\perp}|^2)\cos(\psi_{tr})\, ds' \tag{51}$$

It should be noted that the above same expression (49), can also be employed for computing the coupling efficiency to a plane-wave. For this purpose, one just have to let the beam-waist w_o tend to infinity thus effectively transforming the Gaussian-beam into a plane-wave.

III COMPUTATIONAL RESULTS

In this section we show the computed radiation patterns and efficiencies for the slot feed of fig. 2. The slot length and slot separation are chosen to be $2l = 0.28\lambda$ and $s = 0.16\lambda$ respectively, leading to symmetric patterns with a $-10dB$ beamwidth of around 48^o [2]. The lens is assumed to be a half inch silicon lens ($\epsilon_r = 11.7$) at 500 GHz, corresponding to a radius of about $R = 10.6\lambda$. The hypehemispherical extension length corresponds therefore to $L = R/\sqrt{\epsilon_r} = 3.1\lambda$. On the other hand, when equation (49) is utilized to examine the directivity of the antenna system, maximum gain is found to be achieved at an extension length of $L = 4.0\lambda$ which thus corresponds to the elliptical point [2]. Figures (4) to (11) correspond to the E-plane patterns of the lens antenna system as the slot-feed is sliding off-axis along the $y - axis$, for both the hyperhemisherical and the elliptical extension lengths (see fig. 1). The corresponding H-plane patterns as the slot-feed is sliding along the $x - axis$ are depicted in figure (12) to (19). All patterns are normalized so that $0dB$ corresponds to the angle at which the Gaussian coupling efficiency becomes maximum. The on-axis patterns which are presented in figures (4) and (12) show the typical pattern behavior which consists of a sharper (higher gain) pattern at the elliptical position with a corresponding diffraction-limited phase pattern, in contrast to the quadratic phase pattern at the hyperhemispherical position. As the slot feed moves off-axis, the patterns shift from broadside and in general they deteriorate developing higher sidelobes and becoming asymmetric. For a quantitative examination of the pattern characteristics, the corresponding Gaussian and plane wave efficiencies are shown in figure (20).

The procedure for computing the Gaussian coupling efficiency starts by optimizing the on-axis parameters w_o and z_g of equation (49), for obtaining maximum coupling efficiency (see fig. 3); Let these on-axis optimum parameters denoted by w_{opt} and z_{gop}. As the elementary feed is moving off-axis, the corresponding Gaussian coupling efficiency is computed assuming an icident beam of waist w_{opt} which focuses on a plane parallel to the bottom surface of the lens at a distance z_{gop} from the origin. The direction of incidence denoted by θ_o in figure 3 is optimized for achieving maximum coupling efficiency. The on-axis optimum parameters are computed to be $w_{opt} = 1.17\lambda$, $z_{gop} = 36.5\lambda$ for the hyperhemispherical point corresponding to a Gaussian coupling efficiency of $\eta_G = 98.7\%$, and $w_{opt} = 9.0\lambda$ $z_{gop} = 96\lambda$ for the elliptical point corresponding to $\eta_G = 89.8\%$. The corresponding on-axis coupling efficiencies to a plane-wave are $\eta_P = 4.49\%$ $(23\ dB)$ for the hyphemispherical position and $\eta_P = 78.70\%$ $(35.4\ dB)$ for the elliptical position. In summary, the on-axis characteristics for the coupling efficiencies are as follows:

1. For maximum Gaussian coupling efficiency at the hypehemispherical

position, the incident Gaussian beam should focus on the conjugate point $z_{gop} \sim R\sqrt{\epsilon_r}$, as dictated by ray-optics [3].

2. The hyperhemispherical position couples better to a Gaussian beam than the elliptical position as a consequence of the absence of aberrations when imaging between the two conjugate points [3]. This however comes with a a hefty 13.5 dB reduced gain at the hyperhemispherical position as compared to the elliptical one. Therefore, for the hyperhemispherical position, a second focusing lens should be placed in front of the antenna system in order to increase the overall gain.

3. For the lens system under examination, the difference between the E- and H-plane coupling efficiencies and corresponding parameters is practically negligible.

Now let us also examine what happens when the slot-feed slides off-axis by a distance d_o along the $x-$ or $y-$ axis (see fig. 1). First, the radiated beam shifts from broadside; In the case of the elliptical extension length this shift can easily be predicted using ray-optics and is given by $\tan(\theta_o) \sim d_o/L$. At this angle both the Gaussian coupling efficiency and the coupling to a plane-wave attain their maximum, i.e. the Gaussian coupling effiiency is maximized at the peak of the power pattern. On the other hand, this is no longer true for thr hyperhemispherical point; In this case the peak of the power pattern (maximum coupling to a plane-wave) in general takes place at a smaller angle than the angle of maximum Gaussian coupling efficiency. The maximum Gaussian coupling efficiency is found to be located approximately at the geometrical center of the phase pattern. From coupling figure 20 and from numerical computations, one can also observe the following characteristics:

1. Although the on-axis Gaussian coupling efficiency is higher for the hyperhemispherical position, it rolls off much faster than the elliptical Gaussian coupling efficiency as the slot-feed is moving off-axis.

2. If the Gaussian coupling efficiency is optimized at each off-axis position indpendently of what happens at broadside, then up to a 10% improvement in η_G can be achieved. However, this improvement applies to both the hyperhemispherical and the elliptical positions, making statement 1. always valid.

3. As the slot feed is moving off-axis, the coupling to a plane-wave (directivity) decreases for the elliptical case whereas it increases in the case of the hyperhemispherical position. This is reflected in graphs 4 to 19 which show that the hyperhemispherical pattern becomes sharper as the slot-feed is moving off-axis.

Figure 21 shows the computed reflection loss as the slot-feed is movind off-axis. As shown the loss increases quite significantly with the off-axis distance. This is mainly attributable to total internal reflection which is being quickly establised as the slot-feed moves off-axis. This is especially noticable for the hyperhemispherical extension length where with the feed on-axis, total internal reflection is nowhere taking place on the lens surface.

We close the comments for the numerical results by making a hint for future investigation. It would be very interesting to examine the effect of a thick focusing lens (small f/D) in front of the antenna system. This is particularly interesting for the hyperhemispherical extension length where the gain is low and the off-axis Gaussian coupling efficiency is found rolling off quite significantly.

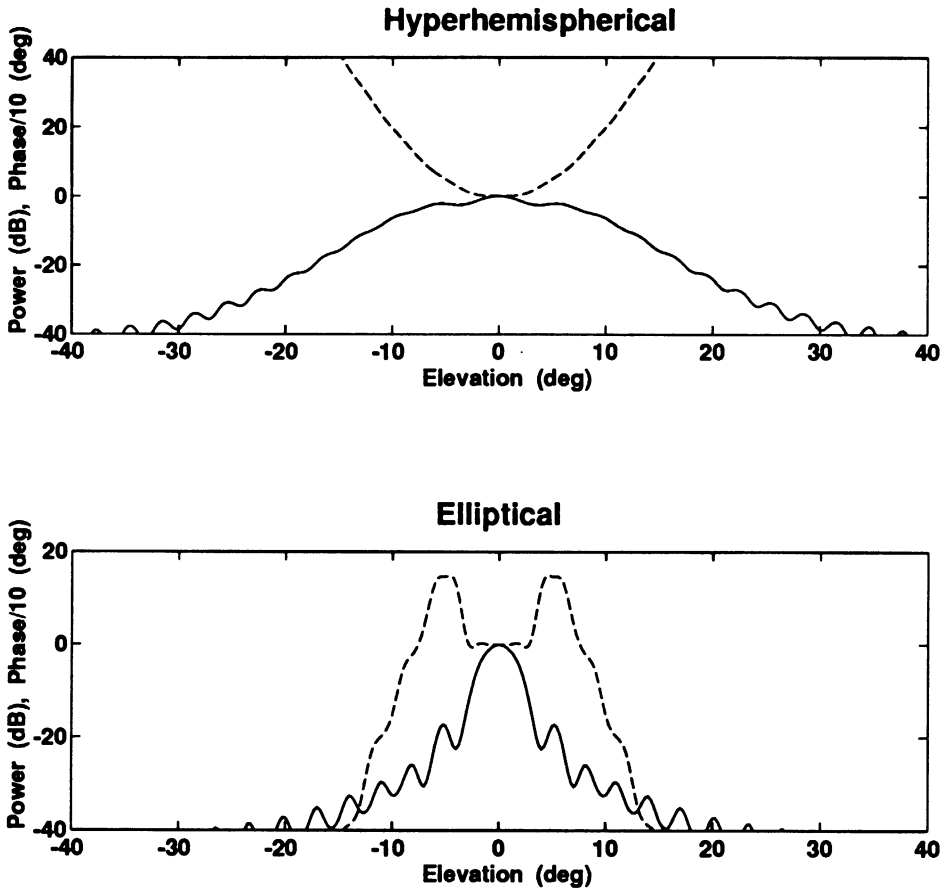

Figure 4: E-plane patterns for the slot-feed located on-axis. The solid line denotes power whereas the dotted phase.

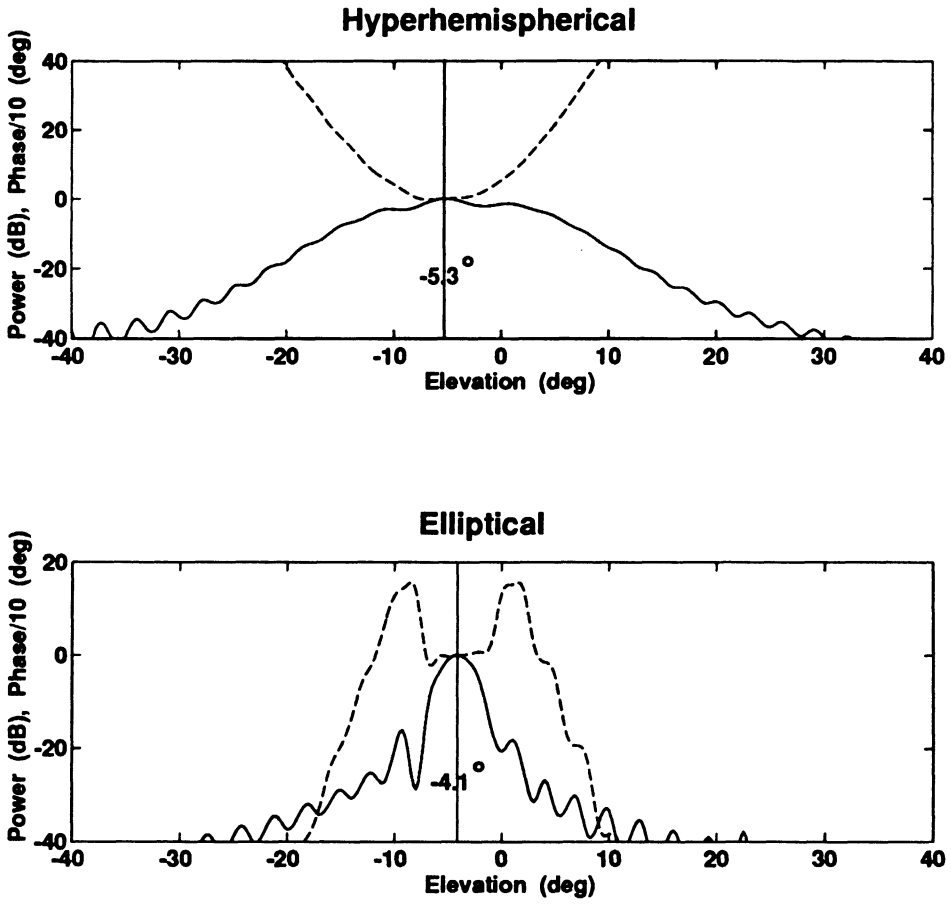

Figure 5: E-plane patterns for the slot-feed shifted by $1\lambda_d$ along the y-axis. The solid line denotes power whereas the dotted phase.

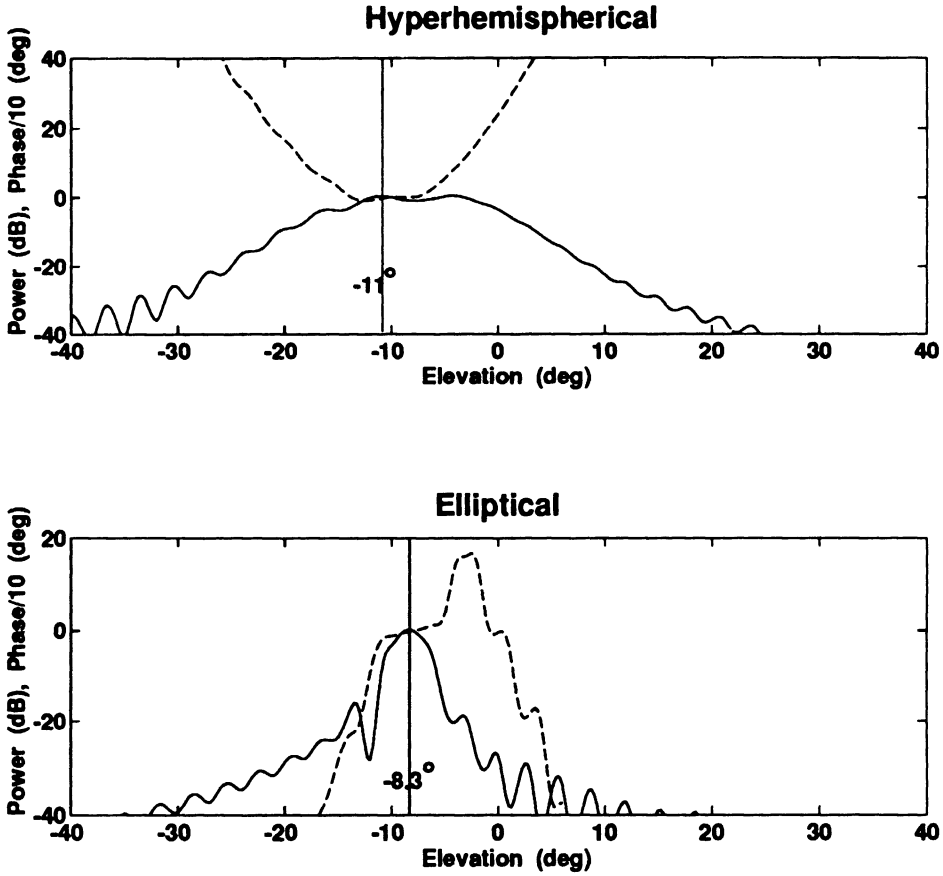

Figure 6: E-plane patterns for the slot-feed shifted by $2\lambda_d$ along the y-axis. The solid line denotes power whereas the dotted phase.

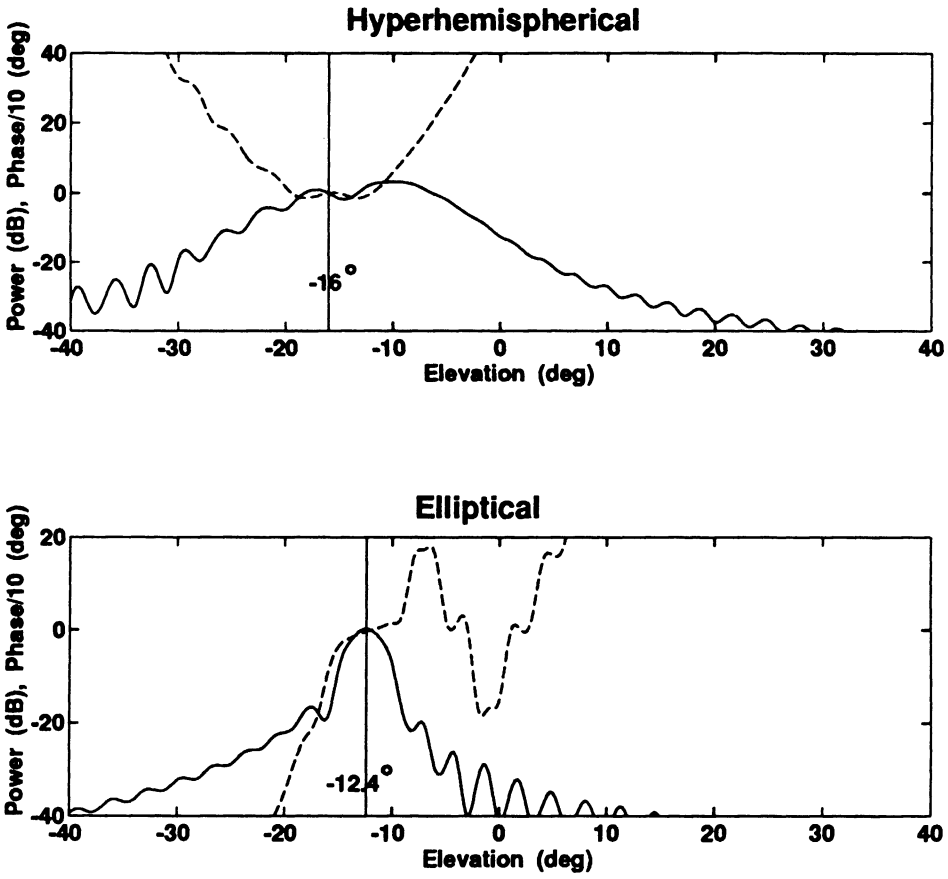

Figure 7: E-plane patterns for the slot-feed shifted by $3\lambda_d$ along the y-axis. The solid line denotes power whereas the dotted phase.

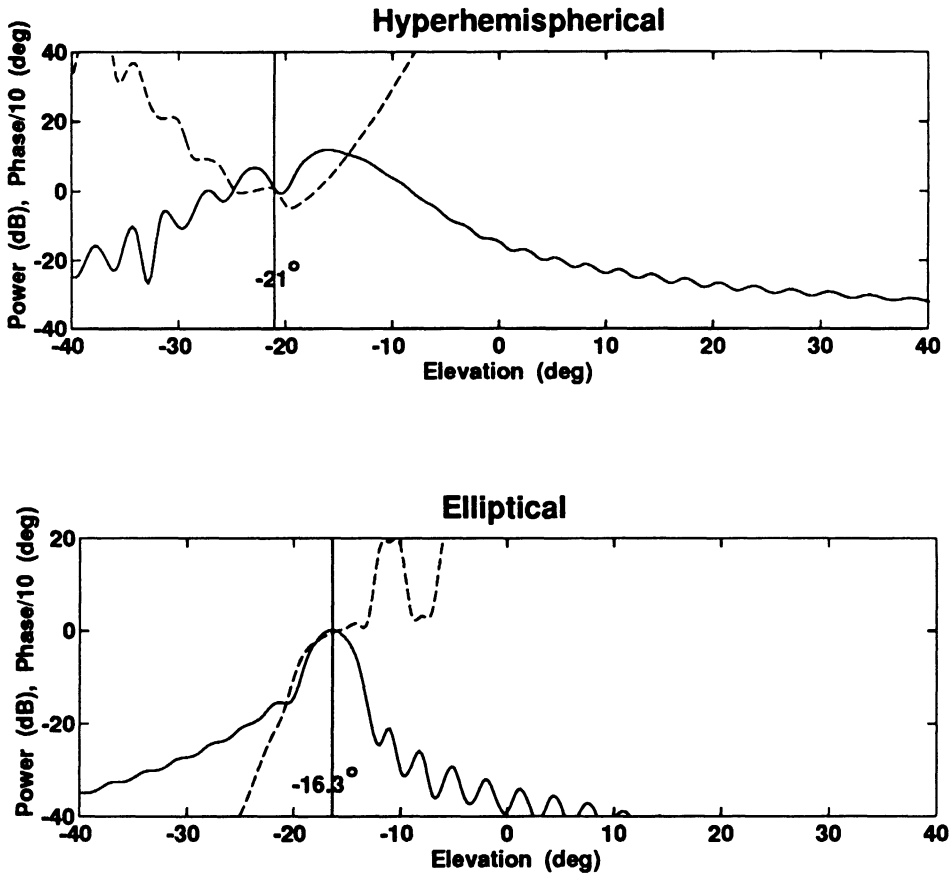

Figure 8: E-plane patterns for the slot-feed shifted by $4\lambda_d$ along the y-axis. The solid line denotes power whereas the dotted phase.

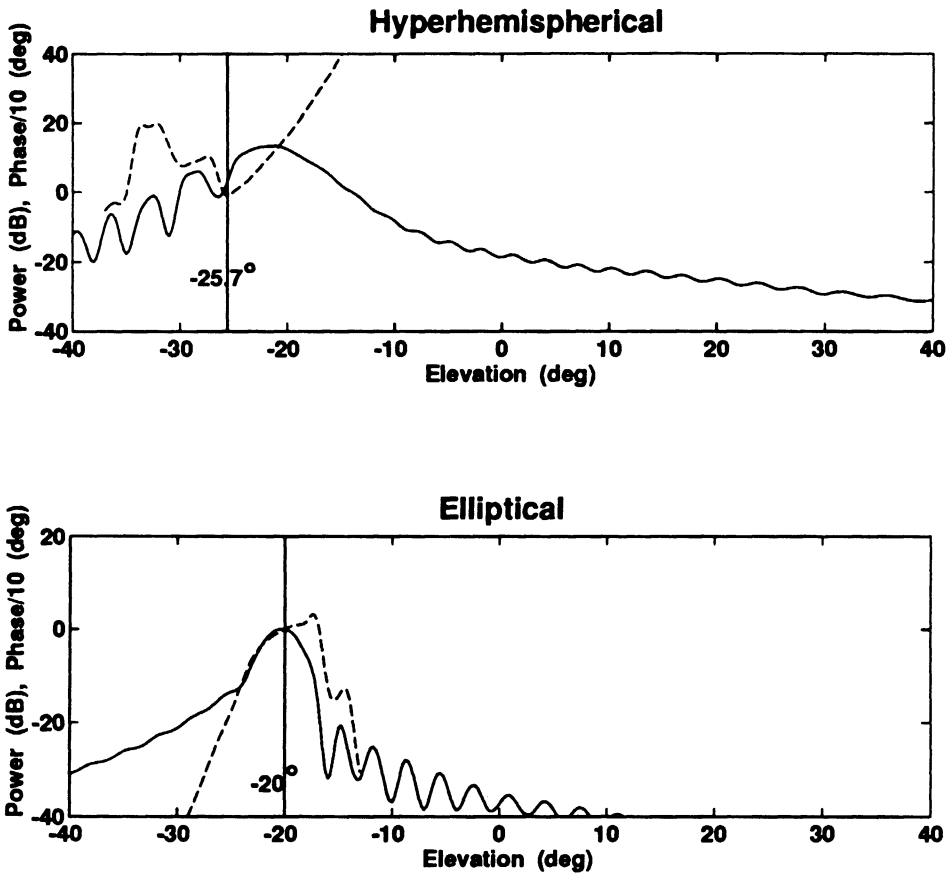

Figure 9: E-plane patterns for the slot-feed shifted by $5\lambda_d$ along the y-axis. The solid line denotes power whereas the dotted phase.

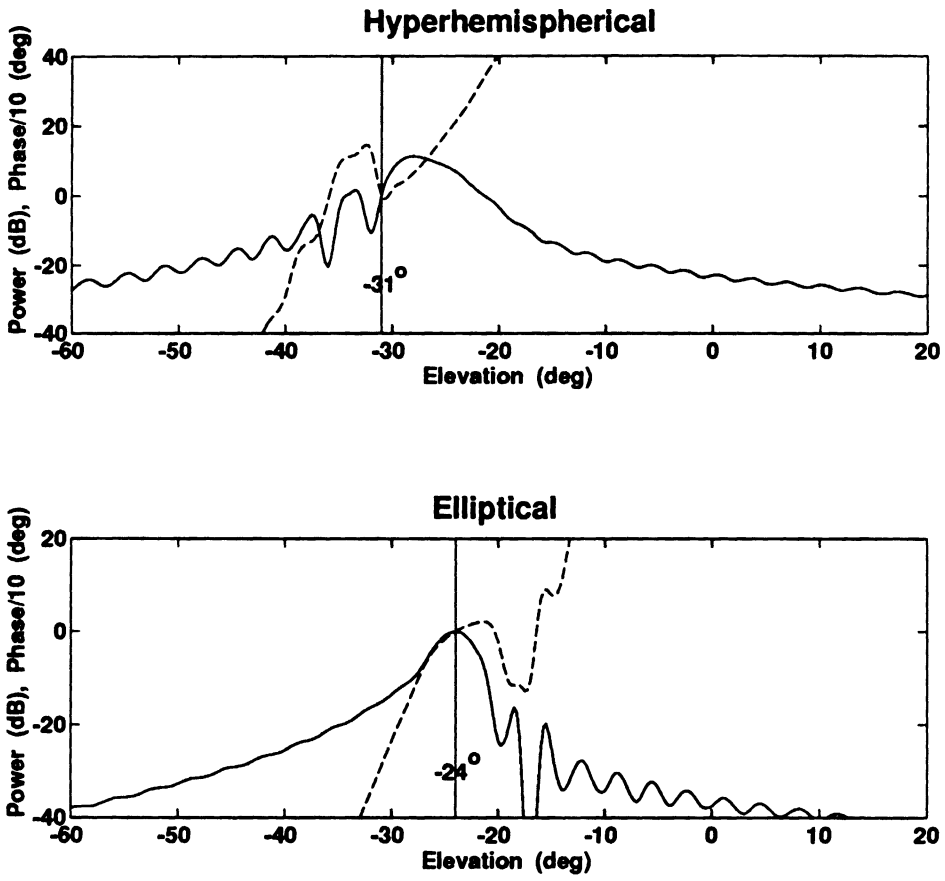

Figure 10: E-plane patterns for the slot-feed shifted by $6\lambda_d$ along the y-axis. The solid line denotes power whereas the dotted phase.

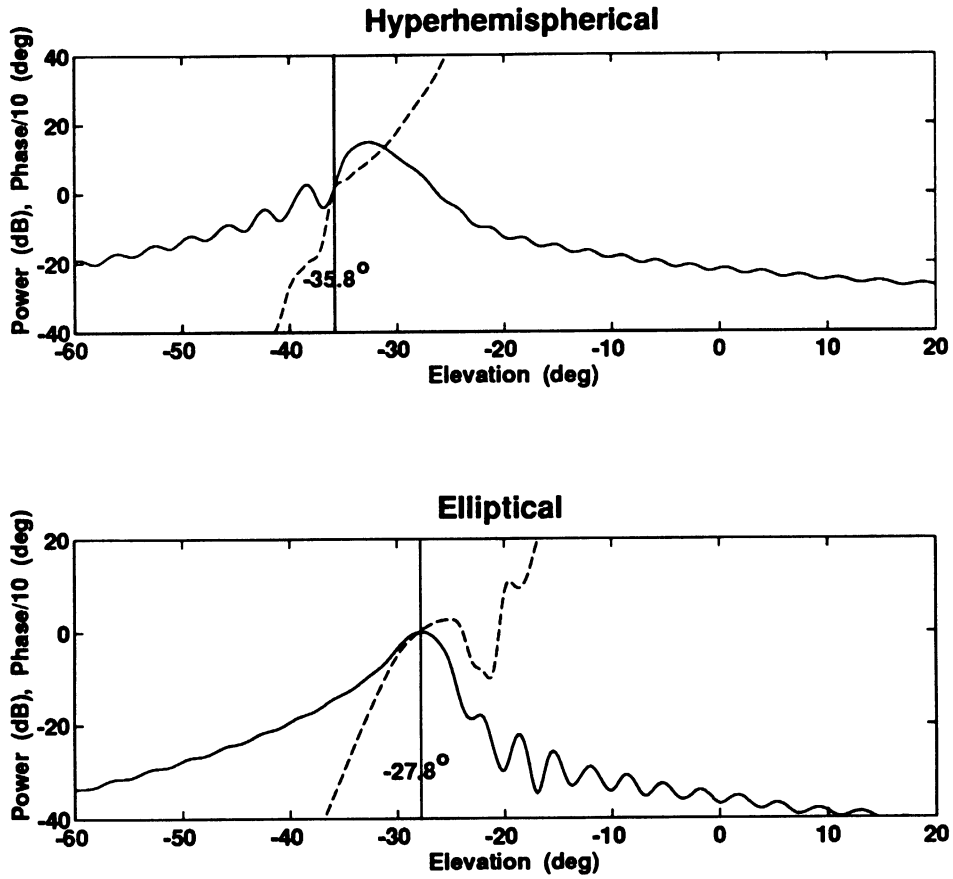

Figure 11: E-plane patterns for the slot-feed shifted by $7\lambda_d$ along the y-axis. The solid line denotes power whereas the dotted phase.

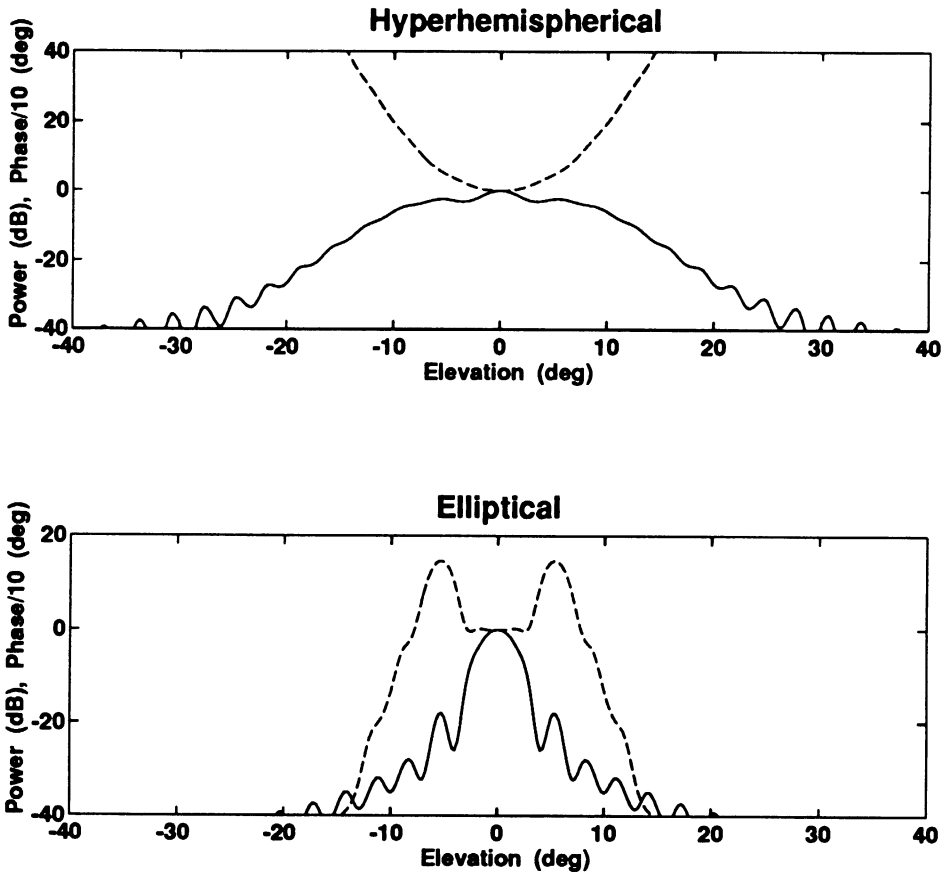

Figure 12: H-plane patterns for the slot-feed located on-axis. The solid line denotes power whereas the dotted phase.

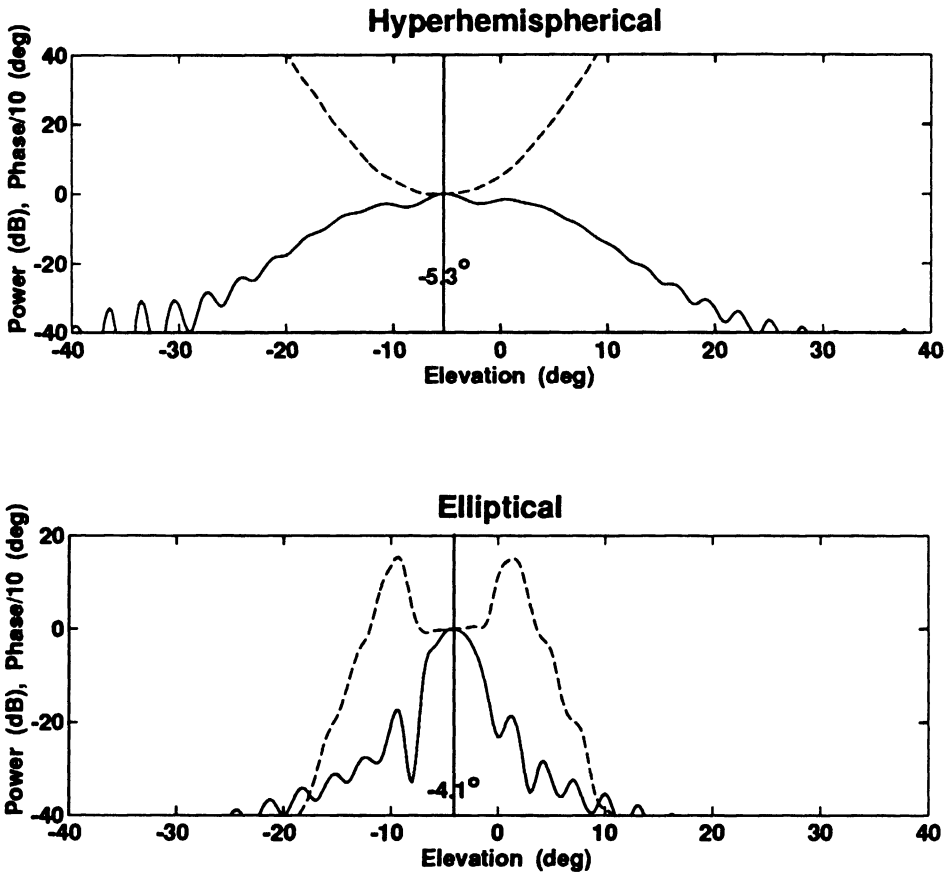

Figure 13: H-plane patterns for the slot-feed shifted by $1\lambda_d$ along the x-axis. The solid line denotes power whereas the dotted phase.

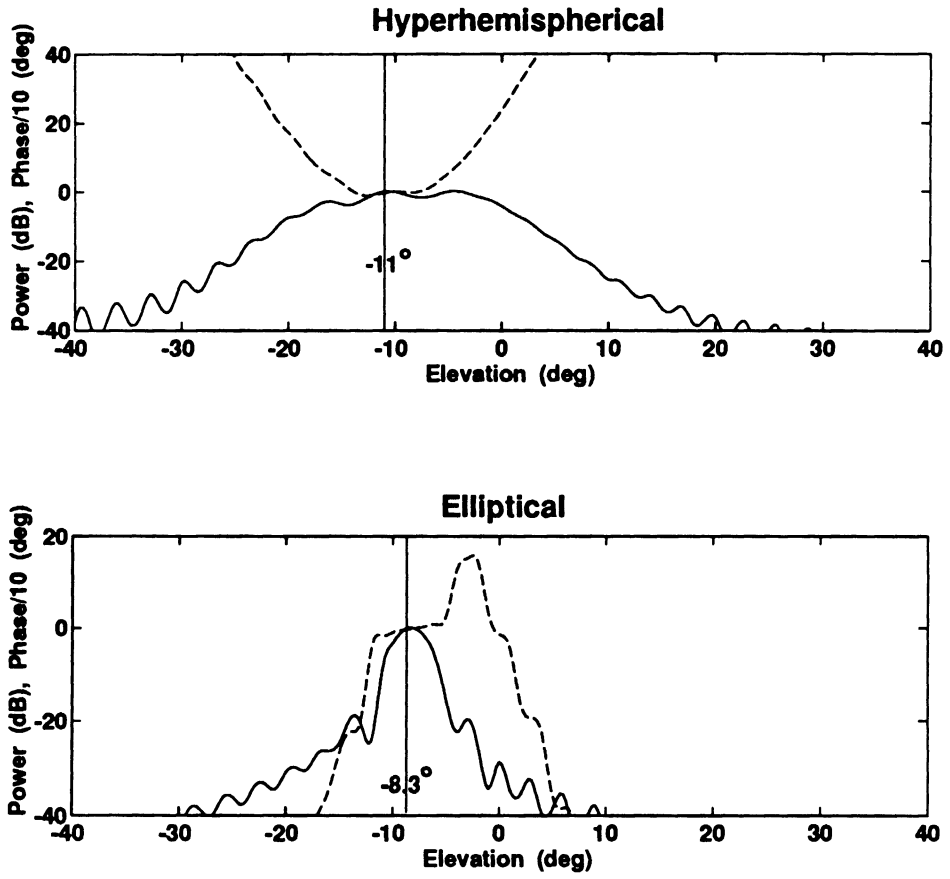

Figure 14: H-plane patterns for the slot-feed shifted by $2\lambda_d$ along the x-axis. The solid line denotes power whereas the dotted phase.

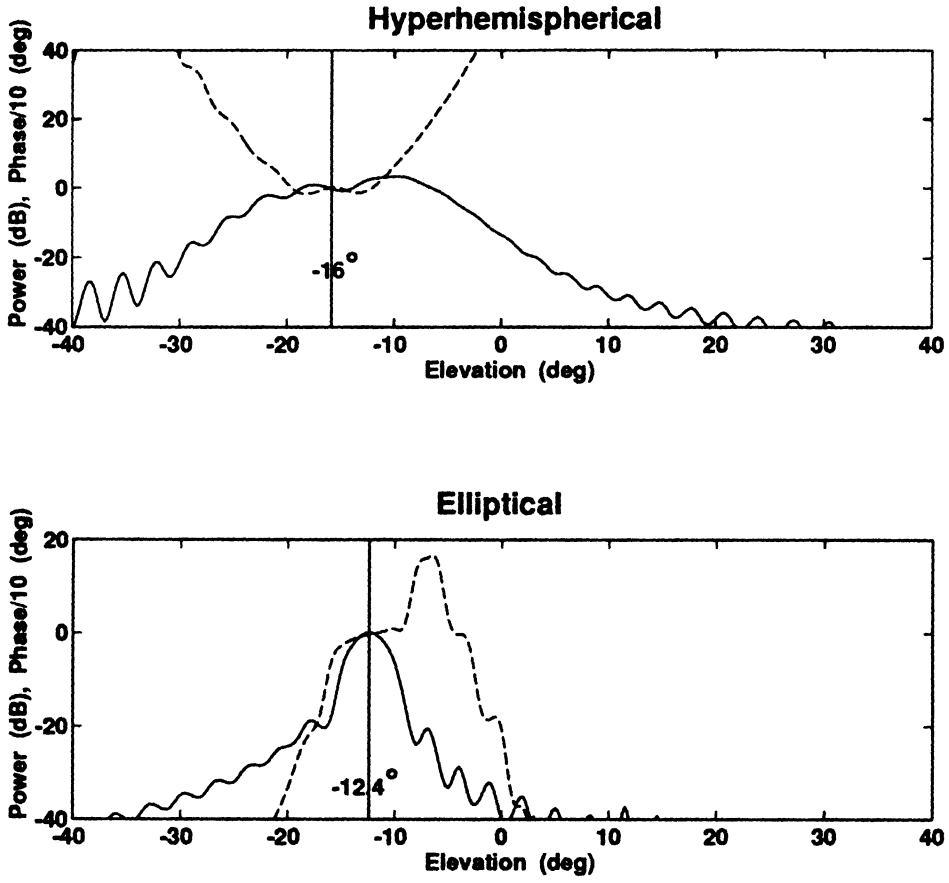

Figure 15: H-plane patterns for the slot-feed shifted by $3\lambda_d$ along the x-axis. The solid line denotes power whereas the dotted phase.

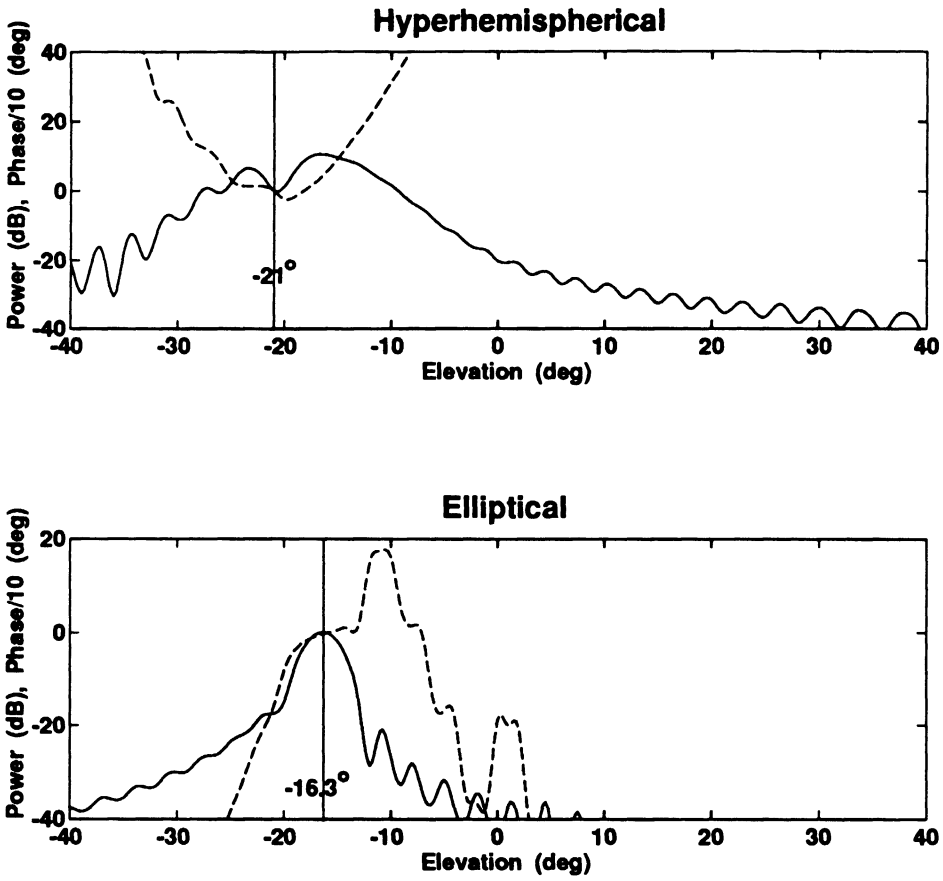

Figure 16: H-plane patterns for the slot-feed shifted by $4\lambda_d$ along the x-axis. The solid line denotes power whereas the dotted phase.

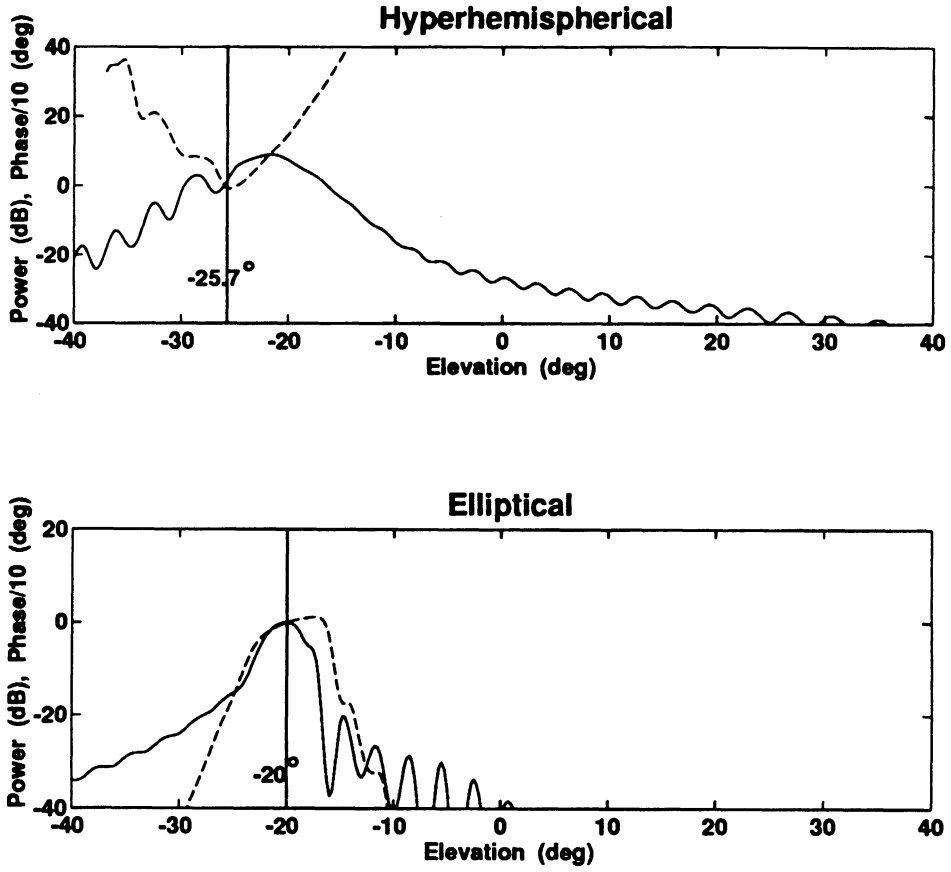

Figure 17: H-plane patterns for the slot-feed shifted by $5\lambda_d$ along the x-axis. The solid line denotes power whereas the dotted phase.

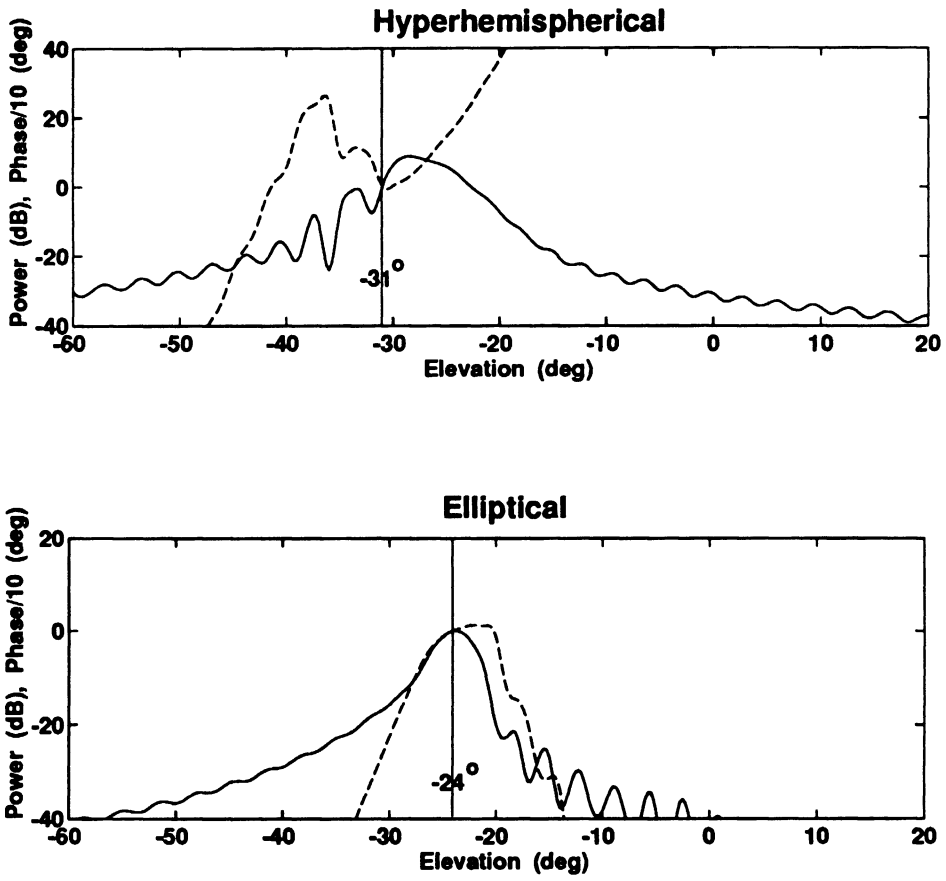

Figure 18: H-plane patterns for the slot-feed shifted by $6\lambda_d$ along the x-axis. The solid line denotes power whereas the dotted phase.

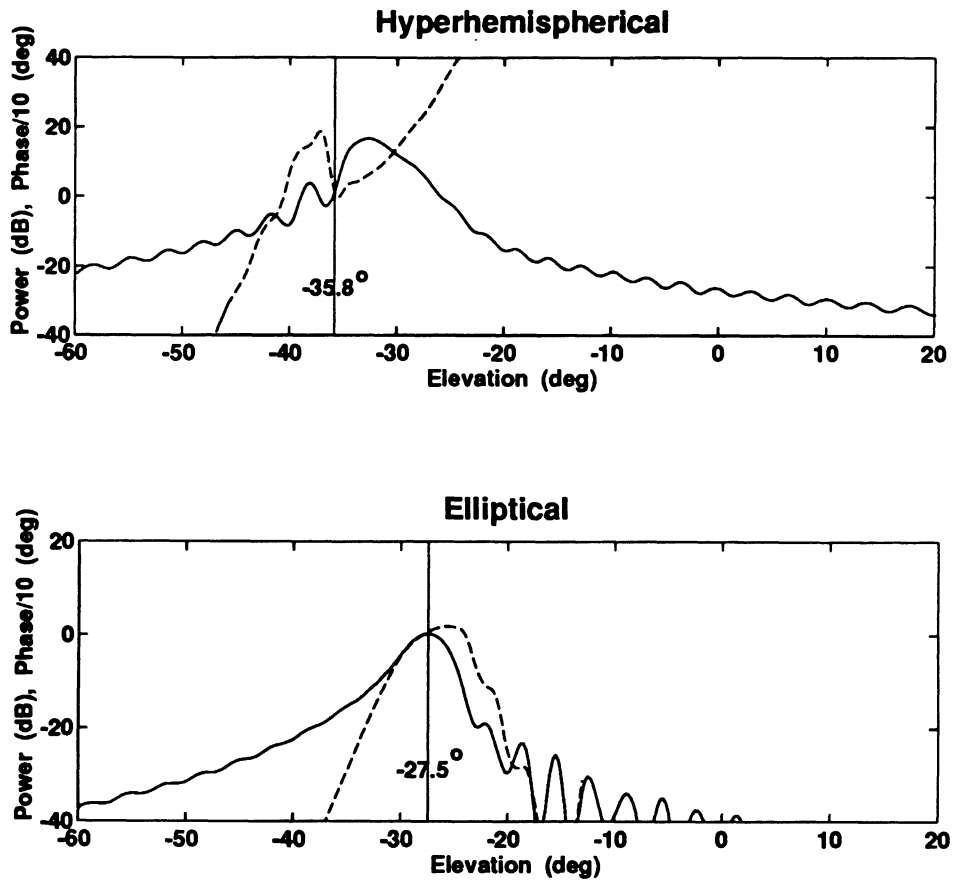

Figure 19: H-plane patterns for the slot-feed shifted by $7\lambda_d$ along the x-axis. The solid line denotes power whereas the dotted phase.

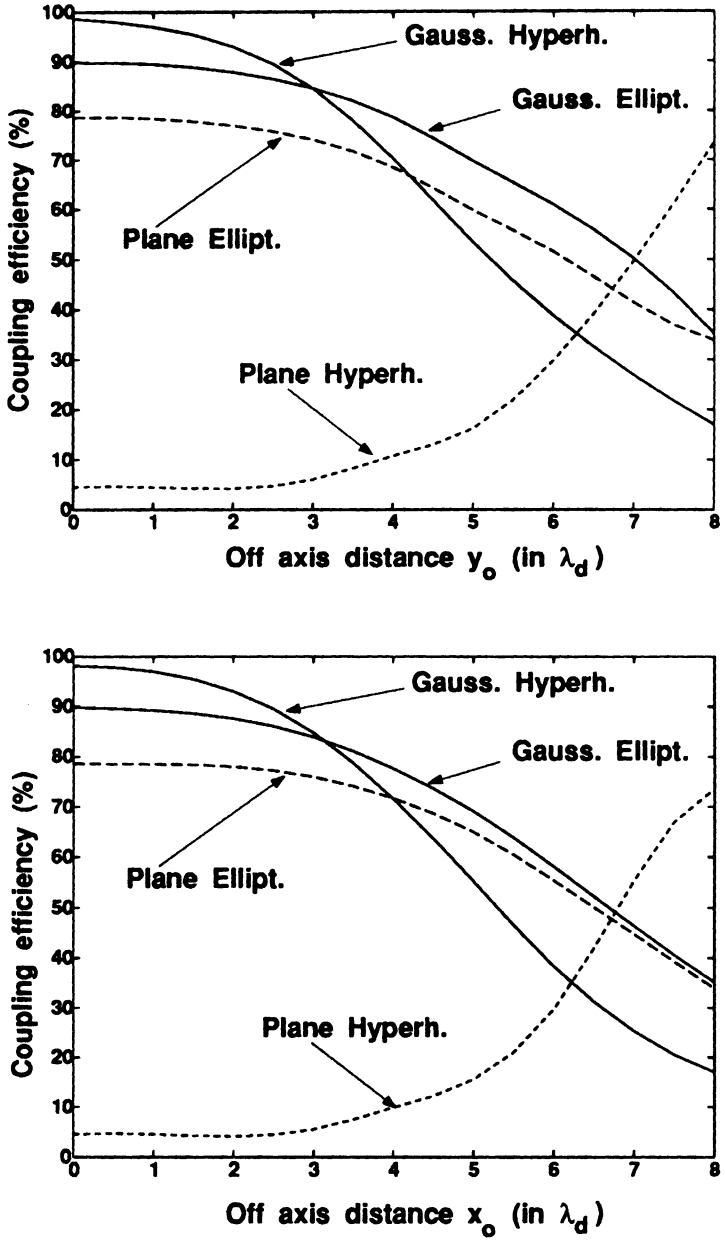

Figure 20: Coupling efficiencies to a Gaussian beam and a plane-wave as a function of the off-axis distance. The upper figure corresponds to the E-plane whereas the lower one to the H-plane

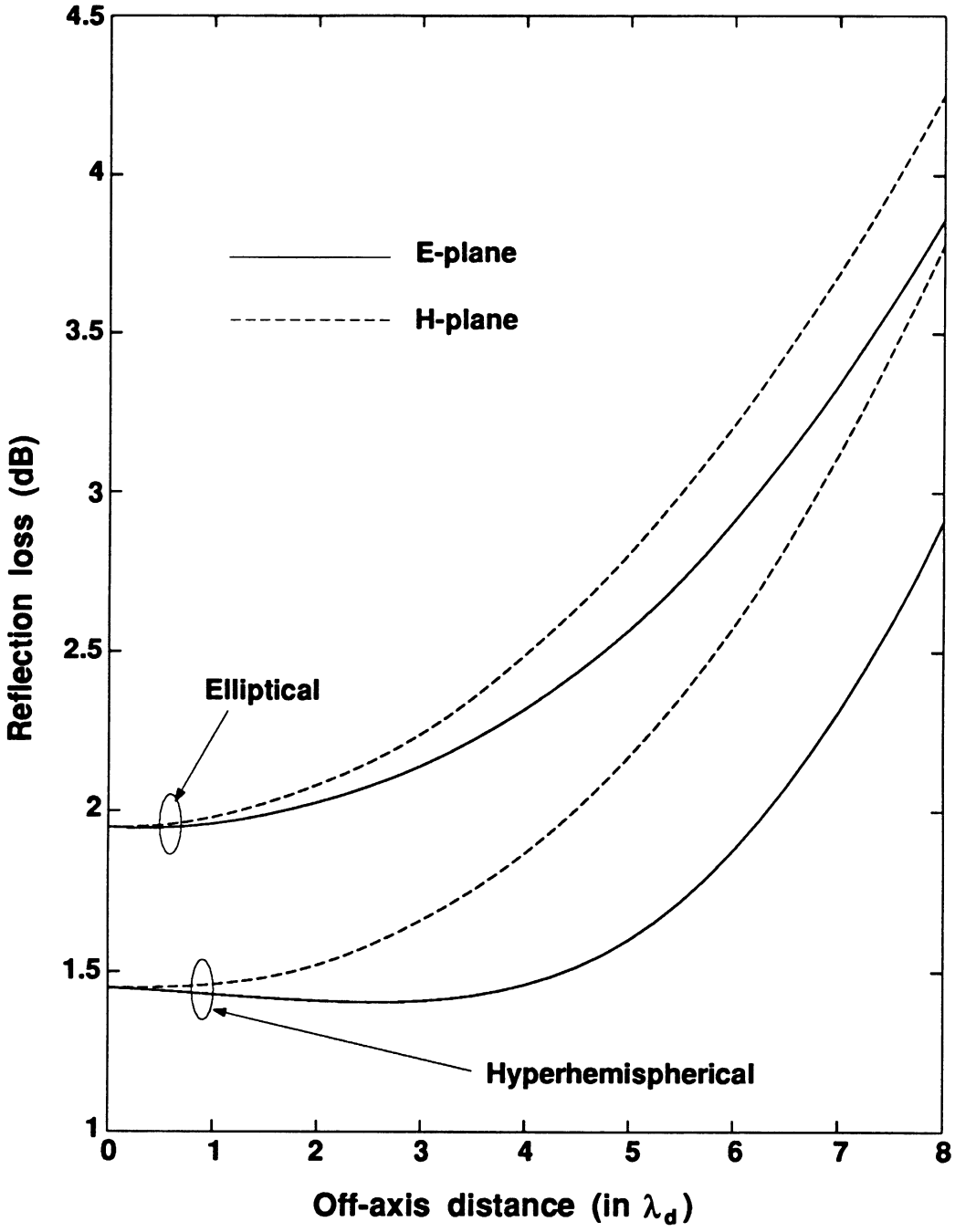

Figure 21: Reflection loss as a function of the off-axis distance.

References

[1] S.E. Schwarz, "Efficiency of Quasi-optical couplers", *Intl. Journal of Infrared and Millimeter Waves*, pp. 1517-1525, vol. 5, 1984.

[2] D.F. Filipovic and G.M. Rebeiz, "Double-Slot antennas on extended hemispherical and elliptical silicon dielectric lenses", *IEEE Trans. on Microwave Theory and Techniques*, Oct. 1993.

[3] M. Born and E. Wolf, "Principles of Optics", Pergamon Press, Oxford, 1964.